Using radon to quantify groundwater discharge and methane fluxes to a shallow, tundra lake on the Yukon-Kuskokwim Delta, Alaska

As Published: https://doi.org/10.1007/s10533-020-00647-w

Publisher: Springer International Publishing

Persistent URL: https://hdl.handle.net/1721.1/131394

Version: Author's final manuscript: final author's manuscript post peer review, without publisher's formatting or copy editing

Using radon to quantify groundwater discharge and methane fluxes to a shallow, tundra lake on the Yukon-Kuskokwim Delta, Alaska

Cite this article as: Jessica S. Dabrowski, Matthew A. Charette, Paul J. Mann, Sarah M. Ludwig, Susan M. Natali, Robert Max Holmes, John D. Schade, Margaret Powell and Paul B. Henderson, Using radon to quantify groundwater discharge and methane fluxes to a shallow, tundra lake on the Yukon-Kuskokwim Delta, Alaska, Biogeochemistry https://doi.org/10.1007/s10533-020-00647-w

Journal: Biogeochemistry

Title: Using radon to quantify groundwater discharge and methane fluxes to a shallow, tundra lake on the Yukon-Kuskokwim Delta, Alaska

Authors: Jessica S. Dabrowski [1,2]*, Matthew A. Charette [2], Paul J. Mann [3], Sarah. M. Ludwig [4], Susan M. Natali [5], Robert Max Holmes [5], John D. Schade [5], Margaret Powell [6], and Paul B. Henderson [2]

[1] Department of Earth and Planetary Sciences, Massachusetts Institute of Technology, 77 Massachusetts Ave, Cambridge, MA 02139, USA; jsdabrow@mit.edu, *ORCID: 0000-0002-3196-4027*;
[2] Department of Marine Chemistry & Geochemistry, Woods Hole Oceanographic Institution, 266 Woods Hole Road, MS#25, Woods Hole, MA 02543, USA; mcharette@whoi.edu; phenderson@whoi.edu;
[3] Department of Geography & Environmental Sciences, Northumbria University, Newcastle upon Tyne, NE1 8ST, UK; paul.mann@northumbria.ac.uk, *ORCID: 0000-0002-6221-3533*;
Department of Earth & Environmental Sciences, Columbia University, 61 Rt. 9W, 207E Oceanography, Palisades, NY 10964, USA; sml2278@columbia.edu; *ORCID: 0000-0002-2873-479X;*
[5] Woods Hole Research Center, 149 Woods Hole Road, Falmouth, MA 02540, USA; snatali@whrc.org, *ORCID: 0000-0002-3010-2994*; rmholmes@whrc.org, *ORCID: 0000-0002-6413-9154*; jschade@whrc.org;
[6] Department of Earth and Planetary Sciences, Harvard University, 20 Oxford St, Cambridge, MA 02138, USA; maggiepowell124@gmail.com;
***** Correspondence: jsdabrow@mit.edu; Tel.: +01-508-289-3850

Abstract: Northern lakes are a source of greenhouse gases to the atmosphere and contribute substantially to the global carbon budget. However, the sources of methane (CH_4) to northern lakes are poorly constrained limiting our ability to the assess impacts of future Arctic change. Here we present measurements of the natural groundwater tracer, radon, and CH_4 in a shallow lake on the Yukon-Kuskokwim Delta, AK and quantify groundwater discharge rates and fluxes of groundwater-derived CH_4. We found that groundwater was significantly enriched (2000%) in radon and CH_4 relative to lake water. Using a mass balance approach, we calculated average groundwater fluxes of 1.2 ± 0.6 and 4.3 ± 2.0 cm d^{-1}, respectively as conservative and upper limit estimates. Groundwater CH_4 fluxes were 7 - 24 mmol m^{-2} d^{-1} and significantly exceeded diffusive air-water CH_4 fluxes (1.3 – 2.3 mmol m^{-2} d^{-1}) from the lake to the atmosphere, suggesting that groundwater is an important source of CH_4 to Arctic lakes and may drive observed CH_4 emissions. Isotopic signatures of CH_4 were depleted in groundwaters, consistent with microbial production. Higher methane concentrations in groundwater compared to other high latitude lakes were likely the source of the comparatively higher CH_4 diffusive fluxes, as compared to those reported previously in high latitude lakes. These findings indicate that deltaic lakes across warmer permafrost regions may act as important hotspots for CH_4 release across Arctic landscapes.

Keywords: radon-222; methane; tundra; groundwater; wetland; subarctic;

Acknowledgements: The authors acknowledge the help of the Polar Field Services Team and helicopter pilot, Stan Herman, for assistance and support in the field. They also thank the other Polaris 2017 and 2018 participants for field assistance, ideas, and companionship. J.S.D. thanks Laura Jardine for sharing her soil samples (B2, U1, U3, B3) (Ludwig et al. 2017a) and to Jordan Jimmie for stream discharge data and sampling. This work was funded by National Science Foundation awards OCE-1458305 to M.A.C., 1561437 to S.M.N, J.D.S., and R.M.H and 1624927 to S.M.N., P.J.M. and R.M.H. We thank the two reviewers for their constructive comments that improved the quality of this manuscript.

1. Introduction

Perennially frozen ground, also known as permafrost, underlies up to 25% of the land in the Northern Hemisphere (Brown et al. 2002). On average, 16% of the terrestrial permafrost landscape is covered by water (Lehner and Döll 2004), and in some areas, like on the Yukon-Kuskokwim Delta in Alaska, it exceeds 30% (US Fish & Wildlife Service 2002). These aquatic systems are closely linked to the terrestrial environment through hydrology. Intense Arctic warming and permafrost thaw may alter the tight connection between terrestrial and aquatic ecosystems. For example, permafrost thaw is causing changes in aquatic systems by changing transit times and shifting flow paths between organic and mineral-rich soils (Vonk et al. 2015).

Groundwater is a source of water and solutes to marine and freshwater systems. In temperate and tropical environments, groundwater discharge has been well-documented as a source of nutrients (Charette and Buesseler 2004; Paytan et al. 2006) and carbon (Beck et al. 2007; Richardson et al. 2017; Kim and Kim 2017) to surface waters. In Arctic environments, there are few studies on groundwater discharge, many of which lack information on quantified fluxes of solutes like carbon and nitrogen (see (Lecher 2017) for a review). Permafrost limits most groundwater flow to the shallow, thawed active layer (Williams 1970; Woo 2012). Potential groundwater supply through sediment beds also depends on the presence or absence of continuous permafrost. Taliks—or perennially unfrozen sediments often found beneath lakes and streams—allow for groundwater exchange between a lake and underlying sediments (Woo 2012). Expanding taliks in a warming climate are expected to enhance exchange between lakes, rivers and underlying aquifers via groundwater supply (Walvoord and Kurylyk 2016).

Many lakes in polar regions are known to be substantial sources of carbon to the atmosphere ((Wik et al. 2016) and references therein), which may be influenced by groundwater-surface water interactions. In addition to delivering dissolved organic carbon that can be mineralized to CO_2 and CH_4, groundwater may directly transport carbon dioxide (CO_2) and methane (CH_4) that was produced in active layer soils to lakes (Kling et al. 1992) where CH_4 can be oxidized or released to the atmosphere. Paytan et al. quantified CH_4 transport to a lake in the Arctic suggesting that carbon-rich soils in the northern latitudes, and the release of carbon from permafrost thaw, provide fuel for CH_4 production (Schuur et al. 2008; Natali et al. 2015; Paytan et al. 2015). With the expected shift to greater subsurface flow due to warming combined with future permafrost thaw (Walvoord and Striegl 2007; Bring et al. 2016; Walvoord and Kurylyk 2016), groundwater may become an increasingly important source of CH_4 to lakes in permafrost environments. This is important in the context of the global

carbon cycle because lakes in the Arctic constitute a substantial portion of Arctic CH_4 sources and represent 6% of global natural CH_4 emissions (Wik et al. 2016).

In this study, we investigated the importance of groundwater as a source of CH_4 to a shallow tundra lake. Radon (^{222}Rn) was used as a natural geochemical tracer of groundwater discharge (Charette et al. 2008; Dimova and Burnett 2011; Dimova et al. 2013), an approach that is advantageous in regions like northern wetlands because it captures groundwater flow despite their low landscape gradients and microtopographic features that inhibit the use of traditional hydrologic methods such as seepage meters and water table elevation measurements (Morison et al. 2017b). In contrast, ^{222}Rn allows for the integration of these heterogeneities. As radon is produced naturally from decay of uranium-series radionuclides in sediments and soils, it is an ideal tracer of all groundwater sources including those present above the permafrost in the seasonally-thawed active layer, in permafrost, and in subpermafrost aquifers (Woo 2012). We used a mass-balance approach (Charette et al. 2008) to quantify groundwater discharge rates and estimate groundwater-derived CH_4 fluxes to the lake and compared them to measured air-water diffusive fluxes and stable isotopes.

2. Materials and Methods

2.1. Study site

The study site (Fig. 1; 61.264 ºN, 163.246 ºW) is located 93 km NW of Bethel, AK in the Yukon Delta National Wildlife Refuge (YDNWR). Fieldwork was conducted over two field seasons from July 1 – 13, 2017 and June 30 – July 10, 2018. The majority of groundwater and lake sampling was conducted in 2017. Gas exchange coefficients and CH_4 air-water fluxes were measured in 2018. Average air temperatures in this region (1981 – 2010 average for Bethel; US National Weather Service) are -0.8 ºC annually, -14.4 ºC in January, 13.4 ºC in July, with above freezing average monthly air temperatures from April to October. Annual precipitation is ~470 mm, with 60 mm occurring in July on average. The average temperatures in July 2017 and 2018, respectively, were 14.4 ºC and 13.9 ºC. The recorded precipitation in July 2017 was 92 mm and in July 2018 was 38 mm (US National Weather Service). The study site is located in a zone of continuous to discontinuous permafrost (Brown et al. 2002) that is moderate in thickness (~180 m) (Ferrians Jr. 1965) with taliks underlying most wetlands and water bodies. Thaw depth was 30 – 40 cm in July 2017 in areas without taliks. The sediments beneath the thick organic layer in this region were deposited in the early Pleistocene (Wilson et al. 2015). This region is characterized by polygonal peat plateaus beside low-lying wetlands. The maximum elevation in this region is approximately 15 meters above sea level and the minimum elevation is approximately 8 m. The elevation of the lake surface and neighboring peat plateaus are 13 and 15 m, respectively.

Lakes and ponds occupy about one third of the YDNWR in surface area (US Fish & Wildlife Service 2002). Most lakes in this region have a maximum depth of <1-3 m (Bartlett et al. 1992) and range widely in surface area from several square meters to several square kilometers. The lake in this study, colloquially termed "Landing Lake," has an average depth of 0.53 ± 0.03 m and a surface area of approximately 0.36 km^2 and is therefore representative of the numerous small, high latitude lakes of the YDNWR. Much of the lake's watershed is in a region of the YDNWR that experienced a wildfire in 2015, as visible by satellite imagery and evident in the field by a lack of vegetation and the presence of leftover charred materials (Fig. 1). Fire frequency has been found to increase with warming in northern Alaska (Higuera et al. 2011) and on the Yukon-Kuskokwim Delta (Sae-Lim et al. 2019), and can cause permafrost thawing, vegetation shifts, and carbon release (Loranty et al. 2016). Although fire effects were not the focus of this study, statistical tests were performed when enough data was available, and potential implications are discussed (Section 4.1.3). Only one surface water channel was connected to Landing Lake at its southeast corner; it was ~0.33 m wide and ~0.15 m deep, and discharge flowed away from the lake at 0.003 $m^3\ s^{-1}$.

2.2. Sample collection

Surface water and groundwater samples for all analyses were collected on July 1 – 12, 2017 and June 30 – July 10, 2018 (Fig. 1, Table 1). Samples from active layer soils and lake and pond bottom sediments were collected in 2017 for analysis and incubation experiments in the laboratory. A lake sediment sample (groundwater symbol next to the weather station, Fig. 1) was collected from the top 5 cm using gloved hands, stored in a clean plastic bag, and frozen until analysis (~4 months). Active layer soils (n = 4, 0 – 30 cm) were cored using a sharpened steel coring barrel, sample tube and hand drill, and then frozen within 48 hours of collection. Samples were thawed for biogeochemical analyses (available online: (Ludwig et al. 2017a)) ~2 weeks after sample collection and refrozen for ~4 months before radionuclide analyses. Air temperature, wind speed and direction, and rainfall rates were collected every 12 minutes using a weather station (AcuRite 5-in-1 Weather Sensor) placed ~5 m above the lake surface on a peninsula (Fig. 1). At each surface water and groundwater sampling event, we measured temperature, dissolved oxygen, and electrical conductivity (YSI 6-Series Sonde (2017), YSI ProPlus multiparameter probe (2018)). Instruments were calibrated immediately prior to fieldwork and in the field.

Lake water samples (2017, n = 18, Table 1) for ^{222}Rn were collected in two ways. A RAD AQUA system (Durridge Inc.; (Schubert et al. 2012)) was used for ^{222}Rn collection for 17 of the samples. One sample, WP4, was collected in a calibrated 2-L plastic bottle with no headspace that was analyzed within four hours. One 100-

L surface water sample (5 20-L "cubitainers") was collected to estimate ^{222}Rn supported by its parent, ^{226}Ra. At the sampling sites in both years, dissolved CH_4 was collected by vigorously shaking 30-mL of the water sample with 30-mL of ambient air for 60 seconds. The headspace was then transferred into pre-evacuated 12-mL Exetainer vials until slightly over-pressurized. Two separate gas samples were collected for separate analyses of CH_4 concentration and $\delta^{13}CH_4$, respectively. Samples for water isotope (δ^2H and $\delta^{18}O$) analysis were also collected in 2017 in 4.5-mL glass vials with no headspace.

Groundwater samples (2017, n = 7, Table 2) were collected from the active layer at 20-40 cm depth below the soil surface using a push-point piezometer (MHE Products, Inc.) and peristaltic pump with gas impermeable tubing. Groundwater samples were limited by the maximum thaw depth of ~40 cm. Samples for ^{222}Rn were collected in 250-mL glass bottles (RAD H2O, Durridge) that were flushed by at least three volumes of sample water and then sealed with no headspace. The same sampling procedures described above for dissolved CH_4 and δ^2H and $\delta^{18}O$ isotopes were used for groundwater samples. One set of water samples was also collected from the southeastern stream discharging Landing Lake for CH_4 and water isotopes (Fig. 1, Table 1).

Spatial and temporal variation in CH_4 flux was examined across Landing Lake in 2018 to provide context for groundwater fluxes of CH_4. Seven chambers were deployed for a 24-hour measurement period around the lake. Gas samples from chamber headspace and dissolved surface water were collected upon chamber deployment and after 12-24 hours (Bastviken et al. 2004). Flux rates were calculated from the difference in initial and final concentrations of CH_4 in the chamber, assuming the flux decreased over time in response to a decreasing concentration gradient between the lake water and chamber headspace (Bastviken et al. 2004). To compare the impact of different flux estimate approaches, instantaneous CH_4 fluxes (averaged triplicate measures, each 5 min duration) were measured during the same period. The CH_4 concentrations in the chamber headspace were measured instantaneously using a Los Gatos Research Ultraportable Greenhouse Gas analyzer, and the increase in concentration over the sampling period was used to calculate chamber fluxes by fitting a linear slope to the data.

2.3. Sample analysis

2.3.1. Radioisotopes

Surface water measurements of ^{222}Rn were conducted in two ways. At all lake sampling locations (except WP4) ^{222}Rn was measured using a radon-in-air monitoring system (RAD7, Durridge) connected to a drying unit, spray chamber (RAD AQUA, Durridge, Inc.) and bilge pump. The temperature in the spray chamber was recorded using a stainless-steel temperature probe and data logger (HOBO U12-008, ONSET). At each station,

the detector was run for 45 – 75 minutes, including 30 minutes of equilibration. Uncertainties (standard errors) were ~3 – 5% for each sample for the integrated measurement periods. The amount of ^{222}Rn in water was calculated using the measured temperature in the spray chamber and its solubility (Dimova and Burnett 2011). At station WP4, ^{222}Rn was measured in a 2-L sample at the field site using the Big Bottle accessory (Durridge) for the RAD7. The uncertainty or standard error for this method was ~16%.

Groundwater ^{222}Rn activities were measured using two different techniques. In the field, groundwater samples (n = 7) were analyzed using the RAD H2O accessory (Durridge, Inc.) within 24 hours of collection. Activities were corrected for decay between collection and measurement times. Uncertainties were 9 – 45 % (1σ, standard error). To determine equilibrium ^{222}Rn activities in groundwater as additional endmembers in the model, soils (n = 4) and lake sediments (n = 1) were incubated in the laboratory (Corbett et al. 1997; Chanyotha et al. 2014). One soil sample (B2, Table 2) was collected >5 km away from the lake, but was included as an endmember due to its similar bulk density to the average bulk density of all other burned soils (Table 3). Radon activities were measured using a radon emanation approach (Key et al. 1979). Efficiencies were determined using a set of radium-fiber standards containing 20 dpm ^{226}Ra (NIST-certified SRM#4967A). Uncertainties were 3 – 15% (1σ, standard error). The ^{222}Rn activities were converted into groundwater endmember activities using porosity and bulk density (Section 2.3.4, Table 3) (Chanyotha et al. 2014).

Experiments in the laboratory were carried out with lake bottom sediments to determine the diffusive flux of ^{222}Rn to the lake. Wet sediments were incubated in gas tight flasks with air stones and radium-free water and connected in a closed loop with two charcoal columns as described by Chanyotha et al. (2016). Radon activities were monitored for 10 – 20 hours. The exponential ingrowth of ^{222}Rn activity was linearly approximated (errors of 4 – 10% at 10 – 25 hours) (Chanyotha et al. 2016). This slope was used to calculate the diffusive flux of ^{222}Rn. Leakage of the system over 20 hours was corrected for using a radium-fiber standard containing 20 dpm ^{226}Ra. A second method was used in which lake bottom sediments were incubated and analyzed with the radon emanation approach described above (Key et al. 1979; Corbett et al. 1997; Chanyotha et al. 2014). The total equilibrium ^{222}Rn activity was multiplied by the decay constant and normalized to the area of the flask to obtain an estimate of the diffusive flux of ^{222}Rn to overlying water. The standard error of 3 trials was reported as the uncertainty. Blanks were run using the same experimental setups and subtracted from any reported values.

To determine the amount of ^{226}Ra dissolved in the Landing Lake that was supporting ^{222}Rn in the water column, the ~100-L sample was filtered onsite at <1 L min^{-1} through a Mn-impregnated acrylic fiber to extract the radium (Moore and Reid 1973). The fiber was analyzed for the activity of ^{222}Rn supported by ^{226}Ra. The

fiber was ashed, packed in a polystyrene vial, and sealed with epoxy to prevent ^{222}Rn loss (Charette et al. 2001). The activity of ^{226}Ra was measured by gamma spectrometry in a well-type germanium gamma detector (Canberra). The detector was calibrated using a ^{226}Ra standard (NIST-certified SRM#4967A) in the same geometry as the sample. The standard error (1σ) was reported as the uncertainty in this measurement.

Table 1. ^{222}Rn activities and dissolved CH_4 concentrations measured at Landing Lake. Latitude (Lat) and longitude (Lon) are in decimal degrees. Depth represents depth of water sample collection. Cond. = conductivity; $\delta^{13}C$ of methane are presented relative to Pee Dee Belemnite (PDB). H_2O stable isotopes reported relative to Vienna Standard Mean Ocean Water (VSMOW). Average value ± standard error is reported. Stream sample not included in average.

Station	Type	Lat.	Lon.	Depth *cm*	Cond *mS cm^{-1}*	O_2 *mg L^{-1}*	Water Temp *°C*	^{222}Rn *dpm m^{-3}*	CH_4 *µmol L^{-1}*	$\delta^{13}C_{CH4}$ ‰	$\delta^{2}H_{H2O}$ ‰	$\delta^{18}O_{H2O}$ ‰
WP4	Lake	61.264	-163.246	10	ND[a]	ND	ND	2700	ND	ND	ND	ND
WP6	Lake	61.265	-163.244	45	0.133	14.7	15.7	2640	ND	ND	ND	ND
WP7	Lake	61.263	-163.244	30	0.066	13.7	17.3	1660	ND	ND	ND	ND
WP8	Lake	61.264	-163.243	30	0.051	14.9	15.6	1140	0.1	-45.7	-67.3	-7.5
WP17	Lake	61.268	-163.240	50	0.072	13.9	16.5	1350	1.4	-47.2	-67.1	-7.1
WP18	Lake	61.267	-163.238	50	0.067	10.0	17.4	1370	1.3	-47.1	-67	-7.3
WP19	Lake	61.268	-163.237	43	0.067	10.7	17.7	1051	1.3	-47.0	-67	-7.3
WP20	Lake	61.270	-163.237	40	0.065	9.5	17.9	1390	1.5	-47.3	-67.1	-7.4
WP21	Lake	61.269	-163.241	44	0.062	12.8	18.1	1080	1.5	-46.3	-67.1	-7.3
WP22	Lake	61.268	-163.243	45	0.062	9.2	18.3	1020	1.3	-41.3	-66.9	-7.4
WP31	Lake	61.263	-163.240	35	0.089	10.0	18.3	1620	1.5	-48.0	-65.7	-7.2
WP32	Lake	61.264	-163.239	35	0.087	10.3	18.9	1394	1.8	-44.6	-65.8	-7.2
WP33	Lake	61.265	-163.238	35	0.080	10.4	19.9	1008	1.6	-46.0	-65.7	-7.2
WP34	Lake	61.266	-163.240	50	0.077	11.1	19.4	570	1.5	-48.7	-65.5	-6.5
WP35	Lake	61.267	-163.243	45	0.072	11.1	19.7	1040	1	-49.2	-65.6	-7.3
WP42	Lake	61.267	-163.246	50	0.076	10.5	15.9	1550	1.7	-47.8	-67.5	-7.5
WP46	Lake	61.265	-163.247	40	0.058	10.6	18.9	1640	6.1	-51.4	-68.8	-8.5
WP47	Lake	61.264	-163.248	50	0.059	10.7	18.7	1650	2.9	-48.5	-67.9	-7
Stream	Stream	61.260	-163.241	10	0.020	6.4	8.5	ND	5.5	-47.0	-87.2	-11.5
Avg.					0.073	11.4	17.9	1400	1.8	-47.1	-66.8	-7.3
±					0.004	0.4	0.3	300	0.5	0.6	0.2	0.1

[a] ND = no data.

Table 2. ^{222}Rn activities and dissolved CH_4 concentrations measured in groundwater and incubated soils. Evidence of the 2015 wildfire is noted for each sample. Depth is below the soil surface. Cond. = conductivity. $\delta^{13}C$ of dissolved CH_4 are presented relative to Pee Dee Belemnite (PDB). H_2O stable isotopes reported relative to Vienna Standard Mean Ocean Water (VSMOW). Average value ± standard error is reported.

Station	Type	Fire[a]	Lat.	Lon.	Depth *cm*	Cond *mS cm^{-1}*	O_2 *mg L^{-1}*	Temp *°C*	^{222}Rn *dpm m^{-3}*	CH_4 *µmol L^{-1}*	$\delta^{13}C_{CH4}$ ‰	$\delta^{2}H$ ‰	$\delta^{18}O$ ‰
WP5	GW[b]	N	61.263	-163.245	30	ND[c]	ND	ND	48000	ND	ND	ND	ND
WP29	GW	Y/N	61.270	-163.237	30	0.085	2.8	5.1	15000	550.8	-73.6	-94.8	-13.2
WT7-3	GW	Y/N	61.270	-163.237	30	0.030	3.3	3.7	35000	7.8	-50.5	-90.9	-13.1
WP43	GW	Y	61.267	-163.247	30	0.186	5.1	16.8	36000	563.2	-58.0	-95.7	-13.2
WP45	GW	Y	61.265	-163.238	40	0.215	5.7	10.4	29000	612.2	-65.2	-106	-14.6
WP30	GW	N	61.270	-163.239	25	0.118	3.2	10.8	ND	456.2	-50.0	-94.0	-14.0
WT8-2	GW	Y	61.270	-163.236	30	0.043	0.9	12.6	ND	25.1	-73.9	-92.1	-12.9
Bottom	Inc[d]	Y/N	61.264	-163.246	0-5	ND	ND	ND	38000	ND	ND	ND	ND
B2-T1	Inc	Y	61.321	-163.243	0-30	ND	ND	ND	5000	ND	ND	ND	ND
U1-T3	Inc	N	61.258	-163.247	0-30	ND	ND	ND	2000	ND	ND	ND	ND
U3-T1	Inc	N	61.270	-163.237	0-30	ND	ND	ND	1000	ND	ND	ND	ND
B3-T2	Inc	Y	61.271	-163.235	0-30	ND	ND	ND	32000	ND	ND	ND	ND
Avg. ±						0.113 ± 0.031	3.5 ± 0.7	9.9 ± 2.0	24000 ± 5000	370 ± 110	-61.9 ± 4.4	-95.6 ± 2.2	-13.5 ± 0.3

[a] Y/N = yes or no for samples collected within the 2015 fire. [b] GW = groundwater. [c] ND = no data. [d] Inc = Incubated soil or sediment. See ref. (Ludwig et al. 2017a) for more details on soil samples B2, U1, U3 and B3.

2.3.2. Methane

Methane concentrations were analyzed using a greenhouse gas chromatograph (Shimadzu GC-2014) at the Woods Hole Research Center, and stable carbon isotopic composition of CH_4 was measured at Northumbria University using a Delta V Plus IRMS interfaced to a Trace Gas Pre-Concentrator and Gas Bench (Thermo Scientific). Each isotope measurement run contained three standards (Liso1, Tiso1, Hiso1; Isometric Instruments), run in full at the beginning and end, with individual standards interleaved throughout (precision <0.5‰). Both CH_4 concentration and isotopic signatures were blank corrected for atmospheric contamination assuming the global mean surface atmospheric CH_4 concentration of 1.8 ppm and $\delta^{13}C$-CH_4 of -47.2‰ (Warwick et al. 2016) and reported relative to Pee Dee Belemnite (PDB).

In 2018, air-water diffusive fluxes (F_{atm}) of CH_4 from the lake were measured directly via the instantaneous and 24-hr measurement period methods described above. From these data, we calculated the gas transfer coefficient (k_x) from the following equation:

$$k_x \text{ (m d}^{-1}) = F_{atm} \text{ (mol m}^{-1} \text{ d}^{-1}) / ([X]_{water} \text{ (mol m}^{-3}) - [X]_{air}), \quad (1)$$

where $[X]_{water}$ is the measured concentration of dissolved CH_4 in the lake, and $[X]_{air}$ is the concentration of CH_4 expected in the lake when in equilibrium with the ambient air (Emerson and Hedges 2008). The equilibrium concentration of CH_4 was calculated using lake temperature, ambient air CH_4 concentration, and Bunsen

solubility constants (Wiesenburg and Guinasso 1979). Two models of gas exchange coefficiencients (k_x) (Crusius and Wanninkhof 2003; Holgerson and Raymond 2016) for the lake was used to derive air-water diffusive fluxes of CH_4 concentrations for Landing Lake in 2017 given similar average wind speed observations for the two years.

2.3.3. $\delta^{18}O$ and $\delta^{2}H$

To examine hydrologic processes and sources of water into the lake, $\delta^{18}O$ and $\delta^{2}H$ stable isotope values of lake water, stream, and groundwater samples were measured at Northumbria University using a Water Isotope Analyzer (LGR LWIA-24d, San Jose, USA). Ratios were measured to a precision of 0.2‰ for $\delta^{2}H$ and 0.03‰ for $\delta^{18}O$ and reported relative to Vienna Standard Mean Ocean Water (VSMOW).

2.3.4. Soil characterization

Porosity and bulk density were measured in order to calculate equilibrium groundwater radon (^{222}Rn) activities (Table 3) (Chanyotha et al. 2014). Soil and sediment were sampled volumetrically, dried at 60° C (organic soils) or 100° C (sediments) for 48 hours, and bulk densities (B_D) calculated as dry mass/volume. Landing Lake bottom sediment characteristics were averaged for the top 5 cm (measured in 0.5 cm intervals, (Ludwig et al. 2017c)). For porosity measurements, soils and sediments were dried in an oven at 50 ºC. Dry sediment/soil was gently packed into a pre-weighed, volume-calibrated test tube. Deionized water was added to the test tube until it just covered the soil surface. The mass of the dry soil and test tube was subtracted from the new mass of the test tube, soil and water. Porosity (φ) was then calculated as follows:

$$\varphi = [\text{Water added (g)} / \text{Density of water (g cm}^{-3})] / \text{Volume of soil (cm}^{3}). \quad (2)$$

After measuring the equilibrium ^{222}Rn activities ($A_{222.\ TOTAL}$) via radon emanation (see section 2.3.1), the following equation was used to calculate groundwater (GW) ^{222}Rn activities (Chanyotha et al. 2014) :

$$\text{GW } ^{222}\text{Rn (dpm m}^{-3}) = [A_{222,\ TOTAL} / \text{wet mass of soil (g)}] \cdot B_D \text{ (g cm}^{-3}) \cdot (1 \text{ cm}^3 / 1 \times 10^{-6} \text{ m}^3) / \varphi. \quad (3)$$

Other soil and sediment characteristics were measured (C, N, moisture, etc.) and can be found online (Ludwig et al. 2017a, c).

2.4. Statistical analyses

Linear regressions were fit to CH_4 and water stable isotope data with a 99% confidence interval. ANOVAs were used to report *p-values* indicating the significance of the relationship. These analyses were performed

across all samples and with the two groups of surface waters and groundwaters, but only statistically significant relationships ($p < 0.05$) were reported.

Although the effects of wildfires on groundwater hydrology and CH_4 are beyond the scope of this study, statistical tests (t-test, two-sample, unequal variances) were performed with sample data to test the potential impacts of the 2015 wildfire. First, the relationship between fire and activities of ^{222}Rn in groundwater samples was examined across all groundwater samples taken during the field campaign, including those not adjacent to Landing Lake (Table 4). The same statistical test was performed for CH_4 in burned and unburned groundwaters. The impact of fire on soil bulk density was also tested using a two-sample t-test, assuming unequal variances for soils collected in 2017 (see data online: (Ludwig et al. 2017a)). Only soils from peat plateaus in 2017 were included to eliminate other environmental variables.

Table 3. Measured soil and sediment characteristics used in the incubation experiments. Visible evidence of the 2015 wildfire is noted for each sample. Sediments were collected from the top 5 cm. Soils were collected from the 0 - 30 cm. Sample names started with B represent burned soils; U, unburned.

Sample name	Type	Fire in 2015?	Porosity	Dry bulk density *g cm^{-3}*	GW ^{222}Rn *dpm m^{-3}*
Bottom Sediment	Landing Lake Sediment	Y/N	0.82	0.45	38000
B2-T1	Soil	Y	0.86	0.19	4800
U1-T3	Soil	N	0.93	0.09	1600
U3-T1	Soil	N	0.90	0.13	1000
B3-T2	Soil	Y	0.74	0.37	32000

3. Results

Water quality data from Landing Lake and nearby groundwaters are presented in Tables 1 and 2. The conductivity of surface water and groundwater was on average 0.073 ± 0.004 and 0.113 ± 0.031 mS cm^{-1}, respectively. All measurements in Landing Lake indicated that it was well oxygenated and thermally well mixed. The average dissolved oxygen concentration was 11.4 ± 0.4 mg L^{-1} (115% saturation). Water temperatures were 15.6 to 19.9 ºC with an average of 17.9 ºC. Groundwater had a lower average dissolved oxygen concentration of 3.5 ± 0.7 mg L^{-1} and a lower average temperature of 9.9 ± 2.0 ºC. The stream outlet of Landing Lake had an intermediate dissolved oxygen concentration of 6.4 mg L^{-1} and a temperature of 8.5 ºC, which was similar to that of groundwater.

3.1. Radioisotopes

Radon activities were ~20 times more enriched in groundwater than in surface water samples (Tables 1 and 2). Groundwater samples in burned soils did not significantly differ with respect to ^{222}Rn compared to other soils ($p = 0.84$, Table 4). However, soils collected in 2017 (see data online: [30]), did significantly differ ($p < 0.01$) in bulk density between recently burned (mean = 0.170 g cm^{-3}, σ^2 = 0.024 g cm^{-3}) and unburned peat plateaus soils (mean = 0.087 g cm^{-3}, σ^2 = 0.005 g cm^{-3}). In the lake, ^{222}Rn activities were on average 1,400 ± 300 dpm m^{-3} (range = 570 – 2,700 dpm m^{-3}) while groundwater activities were 24,000 ± 5,000 dpm m^{-3} (range = 1,000 – 48,000 dpm m^{-3}, Tables 1 and 2). The highest surface water activities were near the southern and western edges of the lake, and the lowest activities were in the center of the lake (Fig. 2a). The lowest radon activities in groundwater were for the three soil samples incubated in the laboratory (Table 2). The measured activity of ^{226}Ra in lake water was 24 ± 2 dpm m^{-3} (standard error) and was a minor contributor to the ^{222}Rn inventory in the lake. The diffusive flux of ^{222}Rn from bottom sediments was 850 ± 90 dpm m^{-2} d^{-1} and 640 ± 90 dpm m^{-2} d^{-1} as found using the hourly flux method (Chanyotha et al. 2016) and equilibration method (Corbett et al. 1997), respectively. The average of the two techniques was 740 ± 140 dpm m^{-2} d^{-1}.

Table 4. Groundwater samples collected in 2017 (including those near Landing Lake and other lakes) and the associated ^{222}Rn activities and methane concentrations. Evidence of fire in 2015 is indicated by Y/N.

Sample name	Type	Fire in 2015?	Lat.	Lon.	Depth *cm*	^{222}Rn *dpm* m^{-3}	CH_4 *µmol* L^{-1}
WP43	GW[1]	Y	61.267	-163.247	30	36000	563.2
WP45	GW	Y	61.265	-163.238	40	29000	612.2
WT8-2	GW	Y	61.270	-163.236	22	ND[2]	25.1
B1-WP27	GW	Y	61.284	-163.247	36	18000	520
B2-WP28	GW	Y	61.273	-163.230	55.5	36000	418.6
B3-WP37	GW	Y	61.284	-163.259	37	19000	ND
B4-WP39	GW	Y	61.284	-163.259	52	32000	628.6
B5-WP40	GW	Y	61.288	-163.262	52	26000	2.9
B2-T1	Inc[3]	Y	61.321	-163.243	0-30	4800	ND
B3-T2	Inc	Y	61.271	-163.235	0-30	32000	ND
WP5	GW	N	61.263	-163.245	30	48000	ND
UB1-WP10	GW	N	61.258	-163.246	45	30000	635.3
UB1-WP15	GW	N	61.258	-163.246	36	25000	517.3
UB2-WP25	GW	N	61.321	-163.238	35	65000	98.4
WP30	GW	N	61.270	-163.239	25	ND	456.2
U1-T3	Inc	N	61.258	-163.247	0-30	1600	ND
U3-T1	Inc	N	61.270	-163.237	0-30	1000	ND
Fire, average						26000	395.8
σ^2						1.07×10^8	7.3×10^4
No fire, average						28000	426.8
σ^2						6.39×10^8	5.4×10^4

[1] GW = groundwater. [2] ND = no data. [3] Inc = incubation (See section 2.3.1) for description of incubation methods.

3.2. Methane

Like radon, dissolved CH_4 was more enriched in groundwater (~200x) than in lake water (Tables 1 and 2). Groundwater samples in burned soils did not significantly differ in dissolved CH_4 compared to unburned soils ($p = 0.85$, Table 4). In the lake, CH_4 varied from 0.1 to 6.1 μmol L^{-1} (Fig. 2b) with an average concentration of 1.8 ± 0.5 μmol L^{-1} (Table 1). The highest concentrations were at stations WP46 and WP47 at the southwestern edge of the lake (Fig. 2b). The lowest concentrations were in the center of the lake. Dissolved CH_4 concentrations in groundwater varied over a larger range from 8 to 612 μmol L^{-1}, and the average groundwater concentration of CH_4 was 370 ± 110 μmol L^{-1} (Table 1). Dissolved CH_4 in the stream was ~5.5 μmol L^{-1}, intermediate between average lake waters and groundwaters.

Dissolved CH_4 in groundwater was on average more depleted in ^{13}C than surface water (-61.9 ± 4.4‰ and -47.1± 0.6‰, respectively; Tables 1 and 2). The most depleted $\delta^{13}C$ value of -51.4‰ in surface water was found at station WP46, coinciding with the highest concentration of CH_4 observed in the lake (Fig. 2b). The stream outlet had a $\delta^{13}C$ value of –47.0‰, similar to lake waters. There was a significant negative relationship between $\delta^{13}C$ and logged CH_4 concentrations in all samples ($\delta^{13}C$ = -5.98 log [CH_4, μmol L^{-1}] – 46.9‰., R^2 = 0.729, $p < 0.01$, Fig. 3); however, this was largely driven by differences between lake and groundwater samples, and there was no detected relationship between $\delta^{13}C$ and dissolved CH_4 within each group ($p > 0.01$).

In 2018, the average CH_4 concentration in Landing Lake was 1.1 ± 0.4 μmol L^{-1} (Table 6), similar to the average in 2017 of 1.8 ± 0.5 μmol L^{-1}. Air-water CH_4 fluxes measured using the instantaneous and 24-hr measurement period methods were 13.5 ± 3.3 mmol m^{-2} d^{-1} and 2.7 ± 1.0 mmol m^{-2} d^{-1}, respectively. The calculated gas exchange coefficients, k_{600}, using the instantaneous and 24-hr measurement period flux methods were 1.32 ± 0.50 m d^{-1} and 0.251 ± 0.014 m d^{-1}, respectively (Table 6).

3.3. $\delta^{18}O$ and $\delta^{2}H$

Stable isotopes of H and O in groundwater were more depleted than lake water (Tables 1 and 2, Fig. 4). Lake water $\delta^{2}H$ and $\delta^{18}O$ values were -66.8 ± 0.2‰ and -7.3 ± 0.1‰, respectively, and groundwater $\delta^{2}H$ and $\delta^{18}O$ values were -95.6 ± 2.2‰ and -13.5 ± 0.3‰, respectively. The stream draining Landing Lake had intermediate $\delta^{2}H$ and $\delta^{18}O$ values, respectively, of -87.2‰ and -11.5‰. When $\delta^{2}H$ values were plotted as a function of $\delta^{18}O$ values (Fig. 4), groundwater samples (Table 2) fell close to the Global Meteoric Water Line (Craig 1961), and were represented by following best-fit line: $\delta^{2}H_{H2O} = 6.87(\delta^{18}O) – 2.90‰$ (R^2 = 0.70, p =

0.04). Stable isotope values for all lake and pond samples collected in 2017 (see data online: (Ludwig et al. 2017b)) were represented by the following relationship: $\delta^2H_{H2O} = 4.31(\delta^{18}O) - 36.55‰$ ($R^2 = 0.96$, $p << 0.01$). Landing Lake surface water samples fell below the GMWL line, but within the range of all lake samples. The stream sample was more depleted than Landing Lake surface waters and was on the line represented by all lakes and ponds.

4. Discussion

4.1. Radon sources and sinks

Consistent with previous studies, ^{222}Rn was much more enriched in groundwater than in surface water (Dimova and Burnett 2011; Dimova et al. 2013; Paytan et al. 2015). Groundwater ^{222}Rn activities (1,000 – 48,000 dpm m^{-3}) were less than those observed in sandy, Floridian soils (~170,000 dpm m^{-3}) (Dimova et al. 2013) and in silty soils near Toolik Lake, Alaska (~490,000 dpm m^{-3}) (Paytan et al. 2015). The lower activity of ^{222}Rn in soils near Landing Lake was likely due to the organic-rich soils that are low in mineral content (by weight) than most sandy or silty soils and therefore lower in its parent isotope ^{238}U that produces ^{222}Rn. The surface water activities (Fig. 2a, 570 – 2,710 dpm m^{-3}) were similar to those reported in a small lake in Florida (1200 – 4800 dpm m^{-3}) (Dimova and Burnett 2011) and Toolik Lake in Alaska (2900 – 5700 dpm m^{-3}) (Paytan et al. 2015).

To quantify groundwater discharge to Landing Lake using ^{222}Rn as a tracer, we constructed a mass balance model that includes all sources and sinks of radon to the lake (Fig. 5). Similar models have been used to study groundwater discharge in both marine and lacustrine environments (Corbett et al. 1997; Dulaiova et al. 2010; Dimova and Burnett 2011; Dimova et al. 2013). The spatial and temporal heterogeneity of groundwater discharge precludes direct quantification; therefore, we use a "flux-by-difference" approach (Charette et al. 2008). Assuming steady state over a few weeks, the change in ^{222}Rn over time should be equal to zero, and the sources must be balanced by the sinks:

$$0 = d^{222}Rn/dt \text{ (dpm } m^{-2} d^{-1}) = F_{222,GW} + F_{226} + F_{benthic} - F_{atm} - \lambda \cdot I_{222} - F_{stream} - F_{recharge}. \quad (2)$$

The sources in this equation other than groundwater ($F_{222,GW}$) of ^{222}Rn include alpha-decay of ^{226}Ra in the water column (F_{226}) and diffusive inputs from lake bottom sediments ($F_{benthic}$). We found no surface water streams entering the lake. The sinks in this model include loss to the atmosphere via gas exchange (F_{atm}), decay ($t_{1/2}$ = 3.82 days), which is equivalent to the inventory of ^{222}Rn (I_{222}) multiplied by its decay constant ($\lambda = 0.181$ $days^{-1}$), and loss via the stream draining Landing Lake (F_{stream}). Recharge of lake water into downgradient soils and sediments ($F_{recharge}$) was not measured, although its potential impact on the mass balance is discussed below.

Sources of uncertainty for each mass balance model term are described in Table 7. Generally, the largest sources of uncertainty in ^{222}Rn mass balances are natural variability in endmember ^{222}Rn activities and atmospheric evasion, as well as mixing with offshore waters for coastal zones (Burnett et al. 2007).

4.1.1. Sinks of ^{222}Rn: gas exchange, decay, streams, and recharge

To determine the loss of radon via gas exchange, two empirical models were compared to field measurements of the gas exchange coefficient at Landing Lake. The air-water flux of radon was calculated using Equation 1 (Emerson and Hedges 2008). In this case, $[X]_{water}$ and $[X]_{air}$ are the activities of radon measured in the lake and the activity expected when the lake is in equilibrium with the atmosphere, respectively. We assumed that atmospheric ^{222}Rn was negligible relative to the lake ^{222}Rn ($[X]_{air}=0$). The gas exchange coefficient, $k_{Rn,}$ was first estimated based on relationships to temperature (Wanninkhof 1992) and wind speed (Crusius and Wanninkhof 2003). For this mass balance, we used the linear relationship for the SF_6 gas exchange coefficient as a function of wind speed (0 – 5 m s^{-1}, 20 ºC) for a lake similar in surface area (0.13 km^2) to Landing Lake (0.36 km^2) (Crusius and Wanninkhof 2003). Then, k_{SF6} (n = 14, (Crusius and Wanninkhof 2003)) was converted to k_{Rn} for the average water temperature in this study (17.9 ± 0.3 ºC) using the appropriate Schmidt numbers ($Sc(SF_6$, 20 ºC) = 956, Sc(Rn, 20 ºC) = 883, Sc(Rn, 17.9 ºC) = 991) (Wanninkhof 1992; Crusius and Wanninkhof 2003). This resulted in the following best-fit linear relationship as a function of wind speed, *u*: k_{Rn}(17.9 ºC, m d^{-1}) = 0.28·*u*(m s^{-1}) - 0.13, which had a slope error of 19%, similar to the 20% error that is typical for empirical wind-speed relationships (Dimova and Burnett 2011). We used the average water temperature (17.9 ± 0.3 ºC, n = 18) and wind speed (3.83 ± 0.05 m s^{-1}, n > 1000) over the 12-day study period, which resulted in an average gas exchange coefficient of k_{Rn} = 1.1 ± 0.2 m d^{-1} and atmospheric flux (F_{atm}) of 1,600 ± 300 dpm m^{-2} d^{-1} (upper limit of gas exchange, Fig. 6).

In another study, an empirical relationship based on surface area, rather than wind speed, across 309 small lakes and ponds over a range of latitudes was used to estimate gas exchange (Holgerson and Raymond 2016). To apply this to Landing Lake, we used the gas exchange coefficient for surface areas of 0.1 – 1 km^2 (k_{600} = 0.80 m d^{-1}) (Holgerson and Raymond 2016) and the Schmidt number for radon at the average lake temperature of 17.9 ± 0.3 ºC (Sc = 991) (Wanninkhof 1992) to obtain a second estimate for the gas exchange coefficient of k_{Rn} = 0.62 m d^{-1}. This produced a lower estimated atmospheric flux (F_{atm}) of 900 ± 200 dpm m^{-2} d^{-1} (lower limit, Fig. 6).

We compared these literature-derived estimates of the gas transfer coefficient with those obtained from direct measurements of gas exchange in 2018 on Landing Lake via 2-min (instantaneous) and 24-hr

measurement floating chambers (Sections 2.2, 2.3.2, Table 6). The coefficients (k_{600}, 12.5 ºC) were 1.3 ± 0.5 and 0.25 ± 0.01 m d^{-1}, respectively, according to each method. When the coefficients were converted for radon at the average lake temperature in 2017, it resulted in values of 1.0 ± 0.4 and 0.20 ± 0.01 m d^{-1}, respectively for k_{Rn} (17.9 ºC). CH_4 concentrations and weather conditions were similar in 2017 and 2018, so we expect these gas exchange coefficients to apply to both years. The instantaneous method resulted in gas transfer coefficients similar to the wind speed model, but was likely influenced by ebullition, resulting in overestimates of the diffusive flux, and thus the gas transfer coefficient. The 24-hr measurement period fluxes were less than both the surface area model and wind speed model, which may have been due to the lower temperature of Landing Lake in 2018 compared to 2017 and the shielding of surface water from wind due to the chamber. To encompass uncertainty due to gas exchange in the ^{222}Rn mass balance, we used the surface area model as a conservative estimate and the wind speed model as an upper limit estimate of groundwater fluxes.

To calculate radon loss from the lake due to decay, we first estimated the inventory of radon in the lake by multiplying the average depth (0.53 ± 0.03 m) by the average activity of ^{222}Rn in the lake (1400 ± 300 dpm m^{-3}, Table 1). The flux due to decay is the product of this inventory and the decay constant ($\lambda \cdot I_{222}$), and was equal to 130 ± 10 dpm m^{-2} d^{-1} (Fig. 6). Of the combined sinks for ^{222}Rn, decay accounted for 8 ± 1% and 13 ± 1%, while atmospheric exchange was 92 ± 18% and 87 ± 17% of total losses of ^{222}Rn, for the upper limit and conservative gas exchange estimates, respectively.

We were not able to directly measure the loss of ^{222}Rn due to recharge or the single stream outlet. However, if we assume negligible evaporation and negligible stream outflow to determine the maximum impact of recharge on the mass balance, we expect that lake water would recharge into adjacent wetland areas at the same rate as groundwater influx (~1 – 4 cm d^{-1}) with a ^{222}Rn activity equal to average lake water (1400 dpm m^{-3}). The ^{222}Rn loss rate for this process would be 20 – 60 dpm m^{-2} d^{-1}, or only 2 – 3% of the combined losses due to decay and gas exchange. In the case of the stream outlet, discharge was ~0.003 m^3 s^{-1}, which is equivalent to 0.07 cm d^{-1} when integrated over the lake's area, as with the other mass balance terms. If the ^{222}Rn activity of the stream is assumed to be that of average lake water (1400 dpm m^3), then the ^{222}Rn loss would be 1.0 dpm m^{-2} d^{-1}, or 0.06 – 0.10% of the combined sinks of decay and gas exchange. Therefore, both recharge and the stream outlet are considered negligible sinks in the ^{222}Rn mass balance, well within the uncertainty of most of the model terms (Table 7).

4.1.2. Sources of ^{222}Rn: dissolved ^{226}Ra, sediments, groundwater

Potential sources of ^{222}Rn in this system other than groundwater are production via decay of dissolved ^{226}Ra and diffusive inputs from bottom sediments (Fig. 5). We first calculated the dissolved inventory of ^{226}Ra by multiplying the measured activity of ^{226}Ra in the lake (24 dpm m^{-3}) by the average depth (0.53 m). The inventory of ^{222}Rn supported by ^{226}Ra is equivalent to the dissolved inventory of ^{226}Ra (12 ± 1 dpm m^{-2}) multiplied by the decay constant of ^{222}Rn. This results in a flux (F_{226}) of 30 ± 2 dpm m^{-2} d^{-1} (Fig. 6). In our steady state model where we assume that sources are equal to sinks, the input of ^{222}Rn from ^{226}Ra can only account for 2 – 3% of the radon inputs to the lake, consistent with other lake ^{222}Rn budgets (Corbett et al. 1997; Dimova et al. 2013).

The diffusive input of ^{222}Rn, which was measured in the laboratory using Landing Lake sediments, agreed well between the two methods. The short-term measurement over 10 – 20 hours resulted in a greater flux than the equilibration method, likely due to the larger concentration gradient between sediment and overlying water for shorter incubation periods. Because the short-term measurement approximates the decay as a linear function, up to 10% error is expected in addition to any experimental error. In the mass balance, we used the average of the two techniques (740 ± 140 dpm m^{-2} d^{-1}) for the sediment-water diffusive flux (Fig. 6). The flux was less than that of freshwater lake sediments from Cambodia (2040 dpm m^{-2} d^{-1}) (Chanyotha et al. 2016), although this is expected because radon is derived from natural uranium in minerals (Charette et al. 2008), and the lake sediments in the YDNWR have a low mineral content. The ^{222}Rn diffusive flux accounted for 42 and 72% of sources in the radon budget for the upper limit and conservative estimates, respectively (Fig. 6). This contribution from diffusion is higher than most lake budgets (Dimova et al. 2013, 2015); since Landing Lake is only ~0.5 m deep, the ratio of bottom sediment area to lake volume is relatively large, which likely explains why diffusion is estimated to be a major contributor to the Landing Lake ^{222}Rn inventory.

Together, diffusive inputs and dissolved ^{226}Ra decay account for 44 to 73% of the sources in the mass balance. Assuming negligible transport of ^{222}Rn out of Landing Lake via recharge and streams (Section 4.1.1), groundwater must be the missing source that contributes 27 to 56% of radon to the lake inventory (Fig. 6).

4.1.3. Quantifying groundwater fluxes

With measurements of groundwater endmembers, one can convert the ^{222}Rn fluxes into groundwater fluxes and volumetric discharge estimates. The remaining 25 ± 10 to 58 ± 24% of the ^{222}Rn inventory was 300 ± 100 to 1000 ± 400 dpm m^{-2} d^{-1}, for the conservative and upper limit estimates, respectively (Fig. 6). In the following equation (Charette et al. 2008),

$$F_{GW}\ (m\ d^{-1}) = F_{222,GW}\ (dpm\ m^{-2}\ d^{-1}) / A_{GW}\ (dpm\ m^{-3}), \quad (3)$$

$F_{222,GW}$ is the flux of ^{222}Rn via groundwater and A_{GW} is the activity of ^{222}Rn in groundwater. There is a significant amount of variability in the groundwater samples when considering both field samples and incubations. ^{222}Rn activities in groundwater at Landing Lake are likely controlled by the mineral content of soils, which is known to increase with depth in peatlands (Morison et al. 2017a). Using the average endmember (Table 2, 24,000 ± 5,000 dpm m^{-3}), the ^{222}Rn flux via groundwater (300 ± 100 to 1000 ± 400 dpm m^{-2} d^{-1}) and Equation 3, we calculated groundwater fluxes of 0.012 ± 0.006 and 0.043 ± 0.020 m d^{-1} (1.2 ± 0.6, 4.3 ± 2.0 cm d^{-1}, Table 5), respectively, for conservative and upper limit estimates. If we use the highest activity endmember (48,000 dpm m^{-3}), the groundwater flux is 0.6 ± 0.3 to 2.1 ± 0.9 cm d^{-1} (Table 5), for conservative and upper limit estimates, respectively. Since these groundwater fluxes were calculated using the average ^{222}Rn inventory for the whole lake surface, they represent inflow averaged over the lake's area. We only have one sample for lake bottom sediment porewater (^{222}Rn = 38,000 dpm m^{-3}) that may be representative of possible subpermafrost groundwater, which is higher in activity that the average groundwater endmember. If subpermafrost groundwater were a significant source of water to this lake, it would likely have a ^{222}Rn activity similar to that of our porewater sample, which is greater than our average groundwater endmember but less than the highest activity endmember; therefore, it would not impact our estimate of ^{222}Rn-based groundwater discharge fluxes. Another factor that could influence these groundwater fluxes is the impact of the 2015 wildfire. Fire did not seem to have a significant impact on ^{222}Rn activities in groundwater, but it did result in significantly higher bulk densities (Table 3). Higher soil density usually lowers hydraulic conductivity, which could cause the groundwater fluxes to be lower in fire-affected areas of the watershed. A dedicated process study would be needed to truly determine the environmental impacts of fire on groundwater hydrology.

The volumetric input of groundwater to the lake of 4,000 ± 2,000 to 15,000 ± 7000 m^3 d^{-1} was estimated by multiplying the groundwater flux (1.2 ± 0.6 to 4.3 ± 2.0cm d^{-1}) by the lake area (3.6 x 10^5 m^2). Such a discharge rate would flush the lake about 3 – 7% by volume per day, equivalent to a residence time of 15 – 53 days (Table 2). For lakes in the US with depths <2 m, residence times on average are 30 – 300 days (Brooks et al. 2014), which agrees well with the residence times calculated here.

Table 5. Estimates of groundwater fluxes, residence times, and methane fluxes for Landing Lake compared to other studies. Average and high activity endmembers refer to the concentrations of radon in groundwater.

Lake name	GW[a] flux *cm d^{-1}*	Residence time *days*	GW [CH_4][b] *μmol L^{-1}*	GW CH_4 flux *mmol m^{-2} d^{-1}*	Lake [CH_4] *μmol L^{-1}*	Air-water CH_4 flux[c] *mmol m^{-2} d^{-1}*
Landing Lake average endmember	1.2 ± 0.6 to 4.3 ± 2.0	12 – 44	370 (8 - 612)	4 ± 2 to 16 ± 7	1.8 ± 0.3	1.3 – 2.3 (1.3 – 5.7)
Landing Lake high activity endmember	0.6 ± 0.3 to 2.1 ± 0.9	25 – 88	370 (8 - 612)	2 ± 1 to 8 ± 3	1.8 ± 0.3	1.3 – 2.3 (1.3 – 5.7)
Toolik Lake (Paytan et al. 2015; Garcia-Tigreros Kodovska et al. 2016)	1.4 ± 0.9	ND[d]	8 – 35 (0.01 – 150)	0.1 – 0.7	0.02 – 0.8	0.06 – 0.2
Northern peatland ponds (n = 38) (Wik et al. 2016)	ND	ND	ND	ND	ND	7 (2 – 10)

[a] GW = groundwater. [b] Average listed along with minimum and maximum in parentheses. Other values listed with entire range of estimates or as average ± standard deviation. [c] Estimated air-water fluxes calculated using Equation 1 and measured air-water fluxes via 24-hr measurement period flux chambers in 2018 listed in parentheses. See Table 6 in Appendix for details. [d] ND = no data.

Unless the lake volumes were increasing over the study period, any groundwater inputs to the lake must be lost to surface water flow, wetland recharge, or evaporation. Surface water flow was estimated to drain only 0.5% of Landing Lake's volume per day, and we had no means to quantify recharge from the lake to the subsurface. If the talik beneath the lake does not penetrate the permafrost completely, the main recharge pathway for water flow would be through the wetland areas near the lake, visible as a darker green color just north and west of the lake (Fig. 1), or through outlet streams. The elevation difference between the plateaus and low-lying areas, such as the lake surface and wetlands, was approximately 2 meters, likely enough to support some level of hydrologic outflow.

Stable isotopes ($\delta^{18}O$ and $\delta^{2}H$ of H_2O) provide quantitative evidence for evaporation at Landing Lake (Fig. 4). All lakes and ponds sampled in 2017 (Ludwig et al. 2017b) fall on the following best-fit line: $\delta^{2}H_{H2O} = 4.31(\delta^{18}O) - 36.55‰$ ($R^2 = 0.96$), which we define as the Local Evaporation Line (LEL). A slope of 4.31 is within modeled slopes of 4 – 6 for lakes at 60ºN (Gibson et al. 2008) and measured slopes of 4.1 – 7.1 in Canadian lakes and wetlands (Gibson et al. 2005). Landing Lake surface waters fell on the LEL and seem to be more impacted by evaporation than the majority of the lakes and ponds sampled, which is expected since Landing Lake had the highest surface area and a similar depth compared to the other sampling sites. The intersection of this evaporation line with the meteoric water line indicates the source of water to the lake (Fontes 1980) was locally sampled active layer groundwaters. Stable isotopes in groundwaters were close to the GMWL and therefore were similar to precipitation. Another study of water stable isotopes in also found that summer precipitation was the major source of water to the active layer on the Alaskan tundra (Throckmorton et al. 2016).

These data show that evaporation was a significant loss of water during the study period, although the exact percentage is not quantifiable with the available data.

4.2. Methane in Landing Lake

Using the radon-derived groundwater fluxes (F_{GW} = 1.2 ± 0.6 to 4.3 ± 2.0 and 0.6 ± 0.3 to 2.1 ± 0.9 cm d^{-1}) and dissolved CH_4 concentration measurements, we estimated groundwater fluxes of CH_4 to Landing Lake from the following equation,

$$F_{CH4,GW}\ (\text{mmol m}^{-2}\ \text{d}^{-1}) = F_{GW}\ (\text{m d}^{-1}) \cdot [CH_4]_{GW}\ (\text{mmol m}^{-3}), \quad (4)$$

in which $F_{CH4,GW}$ is the flux of CH_4 to Landing Lake via groundwater, and $[CH_4]_{GW}$ is the concentration of CH_4 in groundwater (average = 370 μmol L^{-1}). The groundwater flux of CH_4 to Landing Lake ($F_{CH4,GW}$) for July 2017 was 4 ± 2 to 16 ± 7 mmol m^{-2} d^{-1} (High ^{222}Rn endmember: 2 ± 1 to 8 ± 3 mmol m^{-2} d^{-1}, Table 5). A study at Toolik Lake, AK conducted during July in 2011 and 2012, the same time of year as this study, included similar methods to determine radon-derived groundwater fluxes (Paytan et al. 2015). The groundwater flux of CH_4 to Landing Lake is an order of magnitude greater than to Toolik Lake (Table 5, 0.1 – 0.7 mmol m^{-2} d^{-1}), despite having similar groundwater fluxes (Table 5, 1.2 ± 0.6 to 4.3 ± 2.0 cm d^{-1} at Landing Lake; 0.5 – 2.3 cm d^{-1} at Toolik Lake). This is largely due to the greater Landing Lake groundwater CH_4 concentrations (370 μmol L^{-1}) compared to Toolik (21 μmol L^{-1}). These higher fluxes may lead to the observed higher surface water dissolved CH_4 in Landing Lake than at Toolik (Table 5, 1.8 ± 0.3 μmol L^{-1} and 0.02 – 0.8 μmol L^{-1}, respectively). A fraction of CH_4 measured in groundwaters may be oxidized before reaching lake surface waters, and other sources of CH_4, such as methanogenesis in lake sediments may drive the observed differences. Further investigation is recommended to confirm the role that groundwater plays in CH_4 lake budgets.

The depleted carbon-isotopic signature of CH_4 in groundwater (-61.9 ± 4.4‰, Table 2) is consistent with microbial production (Hornibrook et al. 1997; Whiticar 1999), and the large range in isotopic values suggests both methanogenesis and oxidation may be occurring. If oxidation is a dominant process removing CH_4, it is expected that $\delta^{13}C$ will increase logarithmically as CH_4 decreases because lighter CH_4 is preferred in the reaction (Whiticar and Faber 1986; Whiticar 1999), a pattern which was observed in Landing Lake between groundwater and lake water samples (Fig. 3). We assume that the highest concentration of CH_4 observed in groundwater was the starting concentration and stable isotopic composition before any oxidation ($[CH_4]_{GW}$ = 612 μmol L^{-1}, $\delta^{13}C_{CH4,\ GW}$ = -65.2‰, Table 2). The final composition after oxidation was assumed to be the average concentration and stable isotope value in Landing Lake ($[CH_4]_{LAKE}$ = 1.8 μmol L^{-1}, $\delta^{13}C_{CH4,\ LAKE}$ = -47.1‰, Table 1). Following the equation below (Whiticar and Faber 1986):

$$\delta^{13}C_{CH4,\,LAKE} = [\delta^{13}C_{CH4,\,GW} + 1000([CH_4]_{LAKE} / [CH_4]_{GW})^{1/\alpha-1}] - 1000, \quad (5)$$

The fractionation factor (α) between starting groundwater CH_4 and average lake CH_4 was 1.003, in good agreement, considering the margin of error, with the expected α of 1.005 – 1.030 for bacterial CH_4 oxidation (Whiticar 1999), which supports the idea that CH_4 in the lake was produced in the active layer and then transported by groundwater movement, as has been qualitatively observed in other lakes and streams (Kling et al. 1992; Crawford et al. 2013).

Additionally, CH_4 produced in bottom sediments may also be transported into the lake by diffusion and ebullition. Additional measurements of CH_4 concentrations and $\delta^{13}C_{CH4}$ in sediment porewater profiles and floating chambers would be necessary to completely quantify sediment-water diffusive fluxes and ebullitive fluxes, respectively, and their contribution to the lake's CH_4 budget. Diffusion, ebullition and advection may collectively contribute to the CH_4 budget, and each may be impacted by environmental changes. As precipitation increases in the Arctic (Rawlins et al. 2010; Wrona et al. 2016), groundwater flow is expected to increase, impacting advective transport of CH_4 (Walvoord and Kurylyk 2016). Recent work has also revealed that abrupt thaw beneath Arctic lakes can accelerate carbon emissions from lakes (Walter Anthony et al. 2018), potentially increasing future diffusive and ebullitive CH_4 fluxes from sediments.

Once CH_4 enters a lake, it may be lost in the water column via oxidation, to the atmosphere by gas exchange, to groundwater recharge, or surface transport. We calculated diffusive air-water CH_4 (Section 2.3.2), using the observed (1.8 ± 0.3 μmol L^{-1}) and saturated concentrations of CH_4 in the lake (0.004 μmol L^{-1}) and two modeled gas exchange coefficients (k_{CH4} = 1.36 m d^{-1} and 0.79 m d^{-1}, at 17.9 ºC). The flux from Landing Lake to the atmosphere for July 2017 was 1.3 – 2.3 mmol m^{-2} d^{-1}, approximately 3 – 18 times less than lake input of CH_4 via groundwater (Table 5). The 24-hr measurement period CH_4 fluxes in 2018 were 1.3 – 5.7 mmol m^{-2} d^{-1} (Tables 5 and 6), which agreed well with the calculated diffusive air-water fluxes. This suggests that groundwater sources of CH_4 can support all observed diffusion of CH_4 from the lake surface and that they may be a driver of observed diffusive CH_4 emissions.

That the groundwater fluxes of CH_4 were higher than air-water diffusive losses is likely due to the additional removal of CH_4 via oxidation in the water column (Whiticar 1999; Bastviken et al. 2002), a determination supported by $\delta^{13}C_{CH4}$ (Fig. 3). Oxidation of CH_4 in the water column of freshwater lakes is expected by CH_4 oxidizing bacteria (Whiticar 1999) and is typically 30 – 99% of CH_4 produced in sediments or anoxic waters (e.g. (Bastviken et al. 2002, 2008)). Typical oxidation rates can therefore account for this "missing" CH_4 in Landing Lake. Climate warming will increase both methanogenesis and CH_4 oxidation, but

oxidation rates are typically less temperature dependent than production rates, and lower solubility of CH_4 in warmer warmers may cause CH_4 release via bubbles that escape oxidation (Dean et al. 2018).

The air-water diffusive flux in this study was similar to the diffusive methane flux of 2 – 10 mmol m^{-2} d^{-1} for 38 peatland ponds across the Arctic and subarctic (Table 5) (Wik et al. 2016). Another study of 40 lakes in Alaska (~65°N) with similar surface areas found average air-water CH_4 fluxes in summer of 0.6 mmol m^{-2} d^{-1} (Sepulveda-Jauregui et al. 2015). It is important to note that this study was done in the summer season, so these fluxes are likely to change with better temporal coverage. Polar regions are expected to become warmer (Schuur et al. 2008, 2015; Vihma et al. 2016) and wetter (Rawlins et al. 2010; Wrona et al. 2016) over the following decades, so higher CH_4 production in soils is expected if increasing precipitation increases soil moisture (Natali et al. 2015) which can then be transported to aquatic systems by groundwater flow.

In this study, we used naturally occurring ^{222}Rn to quantify groundwater discharge and dissolved CH_4 fluxes to a lake in a subarctic terrestrial wetland. Groundwater fluxes were similar to those at another lake in Alaska measured with the same radon-budget method (Paytan et al. 2015). We found that groundwater is a source of CH_4 to the lake as suggested by the fact that groundwater CH_4 fluxes substantially exceeded diffusive fluxes from the lake surface. The concentrations of CH_4 and diffusive fluxes were higher than the well-studied Toolik Lake. Increased CH_4 production with warming and wetting of the Arctic may lead to higher rates of delivery of CH_4 to aquatic environments due to the combined increase in CH_4 production (Natali et al. 2015) and the shift to greater subsurface flow as permafrost thaws (Walvoord and Kurylyk 2016).

Appendix 1: Methane fluxes

Table 6. The methane concentrations, measured fluxes, and measured gas exchange coefficients for Landing Lake, July 2018. Each method is described in Section 2.2. Average wind speed over the 3 days was 4.6 ± 1.1 m s^{-1}. All measurements were made at the same location (latitude, longitude): 61.26583, -163.24199.

Sample	Method	Length of deployment	Temp. *°C*	Lake CH_4 *µmol* L^{-1}	CH_4 flux *mmol* m^{-2} d^{-1}	k_{600} *m* d^{-1}
7_8	24-hr period	3.6 hr	13.3	2.35	5.7	0.24
7_8	Instantaneous	15 min	13.3	2.35	21.8	0.93
7_9	24-hr period	28.7 hr	12.1	0.93	2.0	0.23
7_9	Instantaneous	15 min	12.1	0.93	6.3	0.71
7_10A	24-hr period	16.6 hr	11.6	0.65	1.8	0.29
7_10A	Instantaneous	15 min	11.6	0.65	17.1	2.32
7_10B	24-hr period	21.4 hr	12.7	0.58	1.3	0.24
7_10B	Instantaneous	15 min	12.7	0.58	17.0	ND[a]
7_10C	Instantaneous	15 min	13.7	ND	5.1	ND

24-hr measurement period average	12.4	1.1	2.7	0.251
±	0.7	0.8	1.0	0.014
Instantaneous average	12.7	1.1	13.5	1.32
±	0.9	0.8	7.4	0.50

[a] ND = no data.

Appendix 2: Uncertainty estimates in the mass balance model

Table 7. The parameters in the mass balance and the methods for estimating the uncertainty in each parameter.

Parameter	Estimation of uncertainty
Gas exchange, Wind Speed Model	Slope error (19%); standard deviation of measured wind speeds (<1%, n > 1000)
Gas exchange, Size Class Model	Estimated at 20% (std error = 7-25% in Holgerson & Raymond, 2016)
Gas exchange, direct measurement	Standard error of measurements (24-37%)
Gas exchange in mass balance	Two estimates: Conservative = Size Class, Upper Limit = Wind Speed; Both errors ~20%
Decay	Standard error of lake ^{222}Rn inventories (11%, n = 18)
Recharge	Impact on mass balance discussed in Section 4.1.1
Stream discharge (out of lake)	Impact on mass balance discussed in Section 4.1.1
Diffusion from bottom sediments	Propagated measurement error of the two methods (19%)
Dissolved ^{226}Ra	Measurement error of ^{226}Ra by gamma spectrometry (8%)
Groundwater ^{222}Rn flux	Propagated uncertainty of all model terms (41%)
Groundwater flux (cm d^{-1})	Reported range for each estimate propagated from: 1) uncertainty of the ^{222}Rn flux (41%); 2) standard error in average groundwater endmember (21%, n = 10) OR measurement error in high activity groundwater endmember (8%)

Author Contributions: Conceptualization, J.S.D., M.A.C., R.M.H, S.M.N, J.D.S. and P.J.M.; methodology, J.S.D., M.A.C. P.J.M., and S.M.L.; validation, J.S.D. and M.A.C.; formal analysis, J.S.D., S.M.L., and M.P.; investigation, J.S.D., P.J.M, S.M.L., M.P., and P.B.H.; resources, J.S.D., P.B.H., M.A.C., R.M.H, S.M.N, J.D.S. and P.J.M.; data curation, J.S.D., S.M.L., P.J.M., and M.P.; writing—original draft preparation, J.S.D.; writing—review and editing, J.S.D, M.A.C., P.J.M, S.M.L, M.P., P.B.H, R.M.H, S.M.N, J.D.S..; visualization, J.S.D.; supervision, M.A.C.; project administration, M.A.C.; funding acquisition, M.A.C., P.J.M, R.M.H, S.M.N, J.D.S..

Conflicts of Interest: The authors declare no conflict of interest. The funders had no role in the design of the study; in the collection, analyses, or interpretation of data; in the writing of the manuscript, or in the decision to publish the results.

References

Bartlett KB, Crill PM, Sass RL, et al (1992) Methane emissions from tundra environments in the Yukon-Kuskokwim delta, Alaska. J Geophys Res 97:16645–16660. doi: 10.1029/91JD00610

Bastviken D, Cole J, Pace M, Tranvik L (2004) Methane emissions from lakes: Dependence of lake characteristics, two regional assessments, and a global estimate. Global Biogeochem Cycles 18:1–12. doi: 10.1029/2004GB002238

Bastviken D, Cole JJ, Pace ML, Van de-Bogert MC (2008) Fates of methane from different lake habitats: Connecting whole-lake budgets and CH4 emissions. J Geophys Res Biogeosciences 113:G02024. doi: 10.1029/2007JG000608

Bastviken D, Ejlertsson J, Tranvik L (2002) Measurement of methane oxidation in lakes: A comparison of methods. Environ Sci Technol 36:3354–3361. doi: 10.1021/es010311p

Beck AJ, Tsukamoto Y, Tovar-Sanchez A, et al (2007) Importance of geochemical transformations in determining submarine groundwater discharge-derived trace metal and nutrient fluxes. Appl Geochemistry 22:477–490. doi: 10.1016/J.APGEOCHEM.2006.10.005

Bring A, Fedorova I, Dibike Y, et al (2016) Arctic terrestrial hydrology: A synthesis of processes, regional effects, and research challenges. J Geophys Res Biogeosciences 121:621–649. doi: 10.1002/2015JG003131

Brooks JR, Gibson JJ, Birks SJ, et al (2014) Stable isotope estimates of evaporation : inflow and water residence time for lakes across the United States as a tool for national lake water quality assessments. Limnol Oceanogr 59:2150–2165. doi: 10.4319/lo.2014.59.6.2150

Brown J, Ferrians Jr. OJ, Heginbottom JA, Melnikov ES (2002) Circum-Arctic Map of Permafrost and Ground-Ice Conditions, version 2. National Snow and Ice Data Center

Burnett WC, Santos IR, Weinstein Y, et al (2007) Remaining uncertainties in the use of Rn-222 as a quantitative tracer of submarine groundwater discharge. In: IAHS-AISH Publication. pp 109–118

Chanyotha S, Kranrod C, Burnett WC (2014) Assessing diffusive fluxes and pore water radon activities via a single automated experiment. J Radioanal Nucl Chem 301:581–588. doi: 10.1007/s10967-014-3157-3

Chanyotha S, Kranrod C, Kritsananuwat R, et al (2016) Optimizing laboratory-based radon flux measurements for sediments. J Environ Radioact 158–159:47–55. doi: 10.1016/j.jenvrad.2016.03.023

Charette M a, Moore WS, Burnett WC (2008) Uranium-and Thorium-Series Nuclides as Tracers of Submarine Groundwater Discharge. Radioact Environ 13:155–191

Charette MA, Buesseler KO (2004) Submarine groundwater discharge of nutrients and copper to an urban

subestuary of Chesapeake Bay (Elizabeth River). Limnol Oceanogr 49:376–385. doi: 10.4319/lo.2004.49.2.0376

Charette MA, Buesseler KO, Andrews JE (2001) Utility of radium isotopes for evaluating the input and transport of groundwater-derived nitrogen to a Cape Cod estuary. Limnol Oceanogr 46:465–470. doi: 10.4319/lo.2001.46.2.0465

Corbett DR, Burnett WC, Cable PH, Clark SB (1997) Radon tracing of groundwater input into Par Pond, Savannah River Site. J Hydrol 203:209–227

Craig H (1961) Isotopic Variations in Meteoric Waters. Science (80-) 133:1702–1703. doi: 10.1126/science.133.3465.1702

Crawford JT, Striegl RG, Wickland KP, et al (2013) Emissions of carbon dioxide and methane from a headwater stream network of interior Alaska. J Geophys Res Biogeosciences 118:482–494. doi: 10.1002/jgrg.20034

Crusius J, Wanninkhof R (2003) Gas transfer velocities measured at low wind speed over a lake. Limnol Oceanogr 48:1010–1017. doi: 10.4319/lo.2003.48.3.1010

Dean JF, Middelburg JJ, Röckmann T, et al (2018) Methane Feedbacks to the Global Climate System in a Warmer World. Rev Geophys 56:207–250. doi: 10.1002/2017RG000559

Dimova NT, Burnett WC (2011) Evaluation of groundwater discharge into small lakes based on the temporal distribution of radon-222. Limnol Oceanogr 56:486–494. doi: 10.4319/lo.2011.56.2.0486

Dimova NT, Burnett WC, Chanton JP, Corbett JE (2013) Application of radon-222 to investigate groundwater discharge into small shallow lakes. J Hydrol 486:112–122. doi: 10.1016/j.jhydrol.2013.01.043

Dimova NT, Paytan A, Kessler JD, et al (2015) Current Magnitude and Mechanisms of Groundwater Discharge in the Arctic: Case Study from Alaska. Environ Sci Technol 49:12036–12043. doi: 10.1021/acs.est.5b02215

Dulaiova H, Camilli R, Henderson PB, Charette MA (2010) Coupled radon, methane and nitrate sensors for large-scale assessment of groundwater discharge and non-point source pollution to coastal waters. J Environ Radioact 101:553–563. doi: 10.1016/j.jenvrad.2009.12.004

Emerson SR, Hedges JI (2008) Chemical Oceanography and the Marine Carbon Cycle. Cambridge University Press, New York

Ferrians Jr. OJ (1965) Permafrost map of Alaska. U.S. Geological Survey Miscellaneous Geologic Investigations Map 445. Scale 1:2,500,000. 1

Fontes JC (1980) Handbook of Environmental Isotope Geochemistry. Elsevier Scientific Pub. Co., New York

Garcia-Tigreros Kodovska F, Sparrow KJ, Yvon-Lewis SA, et al (2016) Dissolved methane and carbon dioxide fluxes in Subarctic and Arctic regions: Assessing measurement techniques and spatial gradients. Earth Planet Sci Lett 436:43–55. doi: 10.1016/J.EPSL.2015.12.002

Gibson JJ, Birks SJ, Edwards TWD (2008) Global prediction of δA and δ2H-δ18O evaporation slopes for lakes and soil water accounting for seasonality. Global Biogeochem Cycles 22:1–12. doi: 10.1029/2007GB002997

Gibson JJ, Edwards TWD, Birks SJ, et al (2005) Progress in isotope tracer hydrology in Canada. Process 19:303–327. doi: 10.1002/hyp.5766

Higuera PE, Chipman ML, Barnes JL, et al (2011) Variability of tundra fire regimes in Arctic Alaska: Millennial-scale patterns and ecological implications. Ecol Appl 21:3211–3226. doi: 10.1890/11-0387.1

Holgerson MA, Raymond PA (2016) Large contribution to inland water CO2 and CH4 emissions from very small ponds. Nat Geosci 9:222–226. doi: 10.1038/ngeo2654

Hornibrook ERC, Longstaffe FJ, Fyfe WS (1997) Spatial distribution of microbial methane production pathways in temperate zone wetland soils: Stable carbon and hydrogen isotope evidence. Geochim Cosmochim Acta 61:745–753. doi: 10.1016/S0016-7037(96)00368-7

Key RM, Brewer RL, Stockwell JH, et al (1979) Some improved techniques for measuring radon and radium in marine sediments and in seawater. Mar Chem 7:251–264. doi: 10.1016/0304-4203(79)90042-2

Kim J, Kim G (2017) Inputs of humic fluorescent dissolved organic matter via submarine groundwater discharge to coastal waters off a volcanic island (Jeju, Korea). Sci Rep 7:7921. doi: 10.1038/s41598-017-08518-5

Kling GW, Kipphut GW, Miller MC (1992) The flux of CO2 and CH4 from lakes and rivers in arctic Alaska. Hydrobiologia 23–36

Lecher A (2017) Groundwater Discharge in the Arctic: A Review of Studies and Implications for Biogeochemistry. Hydrology 4:41. doi: 10.3390/hydrology4030041

Lehner B, Döll P (2004) Development and validation of a global database of lakes, reservoirs and wetlands. J Hydrol 296:1–22. doi: 10.1016/J.JHYDROL.2004.03.028

Loranty MM, Lieberman-Cribbin W, Berner LT, et al (2016) Spatial variation in vegetation productivity trends, fire disturbance, and soil carbon across arctic-boreal permafrost ecosystems. Environ Res Lett 11:. doi: 10.1088/1748-9326/11/9/095008

Ludwig S, Holmes RM, Natali SM, et al (2017a) Polaris Project 2017: Soil fluxes, carbon, and nitrogen, Yukon-

Kuskokwim Delta, Alaska

Ludwig S, Holmes RM, Natali SM, et al (2017b) Polaris Project 2017: Aquatic isotopes, carbon, and nitrogen, Yukon-Kuskokwim Delta, Alaska

Ludwig S, Holmes RM, Natali SM, et al (2017c) Polaris Project 2017: Lake sediment carbon and nitrogen, Yukon-Kuskokwim Delta, Alaska

Moore WS, Reid DF (1973) Extraction of radium from natural waters using manganese-impregnated acrylic fibers. J Geophys Res 78:8880–8886. doi: 10.1029/JC078i036p08880

Morison MQ, Macrae ML, Petrone RM, Fishback L (2017a) Capturing temporal and spatial variability in the chemistry of shallow permafrost ponds. Biogeosciences 14:5471–5485. doi: 10.5194/bg-14-5471-2017

Morison MQ, Macrae ML, Petrone RM, Fishback LA (2017b) Seasonal dynamics in shallow freshwater pond-peatland hydrochemical interactions in a subarctic permafrost environment. Hydrol Process 31:462–475. doi: 10.1002/hyp.11043

Natali SM, Schuur EAG, Mauritz M, et al (2015) Permafrost thaw and soil moisture driving CO2 and CH4 release from upland tundra. J Geophys Res Biogeosciences 120:1–13. doi: 10.1002/2014JG002872.Received

Paytan A, Lecher AL, Dimova N, et al (2015) Methane transport from the active layer to lakes in the Arctic using Toolik Lake, Alaska, as a case study. Proc Natl Acad Sci 112:3636–3640. doi: 10.1073/pnas.1417392112

Paytan A, Shellenbarger GG, Street JH, et al (2006) Submarine groundwater discharge: An important source of new inorganic nitrogen to coral reef ecosystems. Limnol Oceanogr 51:343–348. doi: 10.4319/lo.2006.51.1.0343

Rawlins MA, Steele M, Holland MM, et al (2010) Analysis of the Arctic System for Freshwater Cycle Intensification: Observations and Expectations. J Clim 23:5715–5737. doi: 10.1175/2010JCLI3421.1

Richardson CM, Dulai H, Popp BN, et al (2017) Submarine groundwater discharge drives biogeochemistry in two Hawaiian reefs. Limnol Oceanogr 62:S348–S363. doi: 10.1002/lno.10654

Sae-Lim J, Russell JM, Vachula RS, et al (2019) Temperature-controlled tundra fire severity and frequency during the last millennium in the Yukon-Kuskokwim Delta, Alaska. Holocene. doi: 10.1177/0959683619838036

Schubert M, Paschke A, Bednorz D, et al (2012) Kinetics of the water/air phase transition of radon and its implication on detection of radon-in-water concentrations: Practical assessment of different on-site radon

extraction methods. Environ Sci Technol 46:8945–8951. doi: 10.1021/es3019463

Schuur EAG, Bockheim J, Canadell JG, et al (2008) Vulnerability of Permafrost Carbon to Climate Change : Implications for the Global Carbon Cycle. Bioscience 58:701–714

Schuur EAG, McGuire AD, Schädel C, et al (2015) Climate change and the permafrost carbon feedback. Nature 520:171–179. doi: 10.1038/nature14338

Sepulveda-Jauregui A, Walter Anthony KM, Martinez-Cruz K, et al (2015) Methane and carbon dioxide emissions from 40 lakes along a north-south latitudinal transect in Alaska. Biogeosciences 12:3197–3223. doi: 10.5194/bg-12-3197-2015

Throckmorton HM, Newman BD, Heikoop JM, et al (2016) Active layer hydrology in an arctic tundra ecosystem: quantifying water sources and cycling using water stable isotopes. Hydrol Process 30:4972–4986. doi: 10.1002/hyp.10883

US Fish & Wildlife Service (2002) Yukon Delta National Wildlife Refuge. In: Fact Sheet. https://www.fws.gov/uploadedFiles/Region_7/NWRS/Zone_1/Yukon_Delta/PDF/yukondelta.pdf. Accessed 24 Jul 2018

Vihma T, Screen J, Tjernström M, et al (2016) The atmospheric role in the Arctic water cycle: A review on processes, past and future changes, and their impacts. J Geophys Res Biogeosciences 121:586–620. doi: 10.1002/2015JG003132

Vonk JE, Tank SE, Bowden WB, et al (2015) Reviews and syntheses: Effects of permafrost thaw on Arctic aquatic ecosystems. Biogeosciences 12:7129–7167. doi: 10.5194/bg-12-7129-2015

Walter Anthony K, Schneider von Deimling T, Nitze I, et al (2018) 21st-century modeled permafrost carbon emissions accelerated by abrupt thaw beneath lakes. Nat Commun 9:3262. doi: 10.1038/s41467-018-05738-9

Walvoord MA, Kurylyk BL (2016) Hydrologic Impacts of Thawing Permafrost—A Review. Vadose Zo J 15:1–20. doi: 10.2136/vzj2016.01.0010

Walvoord MA, Striegl RG (2007) Increased groundwater to stream discharge from permafrost thawing in the Yukon River basin: Potential impacts on lateral export of carbon and nitrogen. Geophys Res Lett 34:. doi: 10.1029/2007GL030216

Wanninkhof R (1992) Relationship Between Wind Speed and Gas Exchange. J Geophys Res 97:7373–7382

Warwick NJ, Cain ML, Fisher R, et al (2016) Using δ13C-CH4 and δD-CH4 to constrain Arctic methane emissions. Atmos Chem Phys 16:14891–14908. doi: 10.5194/acp-16-14891-2016

Whiticar MJ (1999) Carbon and hydrogen isotope systematics of bacterial formation and oxidation of methane. Chem Geol 161:291–314. doi: 10.1016/s0009-2541(99)00092-3

Whiticar MJ, Faber E (1986) Methane oxidation in sediment and water column environments - Isotope evidence. Org Geochem 10:759–768. doi: 10.1016/S0146-6380(86)80013-4

Wiesenburg DA, Guinasso NL (1979) Equilibrium solubilities of methane, carbon monoxide, and hydrogen in water and sea water. J Chem Eng Data 24:356–360. doi: 10.1021/je60083a006

Wik M, Varner RK, Anthony KW, et al (2016) Climate-sensitive northern lakes and ponds are critical components of methane release. Nat. Geosci. 9:99–105

Williams JR (1970) Ground water in the permafrost regions of Alaska

Wilson FH, Hults CP, Mull CG, Karl SM (2015) Geologic Map of Alaska. USGS Scientific Investigations Map 3340, pamphlet

Woo MK (2012) Permafrost hydrology. Springer

Wrona FJ, Johansson M, Culp JM, et al (2016) Transitions in Arctic ecosystems: Ecological implications of a changing hydrologic regime. J Geophys Res Biogeosciences 121:650–674. doi: 10.1002/2015JG003133

Journal: Biogeochemistry

Title: Using radon to quantify groundwater discharge and methane fluxes to a shallow, tundra lake on the Yukon-Kuskokwim Delta, Alaska

Authors: Jessica S. Dabrowski [1,2]*, Matthew A. Charette, Paul J. Mann, Sarah. M. Ludwig, Susan M. Natali, Robert Max Holmes, John D. Schade, Margaret Powell, and Paul B. Henderson

*****Affiliation and correspondence: jsdabrow@mit.edu; Tel.: +01-508-289-3850

[1] Department of Earth and Planetary Sciences, Massachusetts Institute of Technology, 77 Massachusetts Ave, Cambridge, MA 02139, USA; jsdabrow@mit.edu, *ORCID: 0000-0002-3196-4027*;

[2] Department of Marine Chemistry & Geochemistry, Woods Hole Oceanographic Institution, 266 Woods Hole Road, MS#25, Woods Hole, MA 02543, USA; mcharette@whoi.edu; phenderson@whoi.edu;

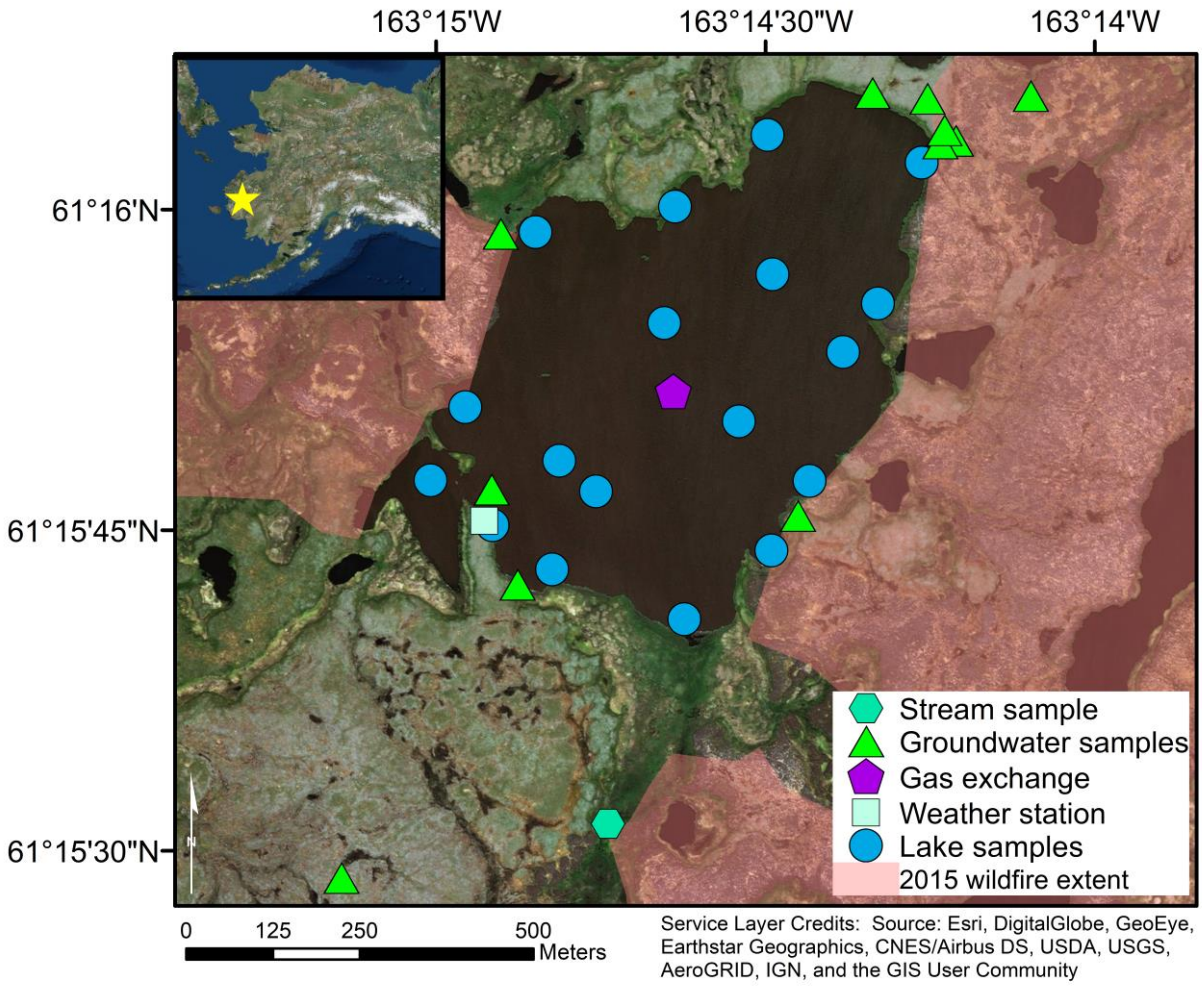

Fig. 1 "Landing Lake" sampling locations and the study site location within Alaska, USA shown in inset (star symbol). One groundwater sample (B2) is not shown because it was 5 km north of Landing Lake (Figure was made using ArcMap 10.5.1).

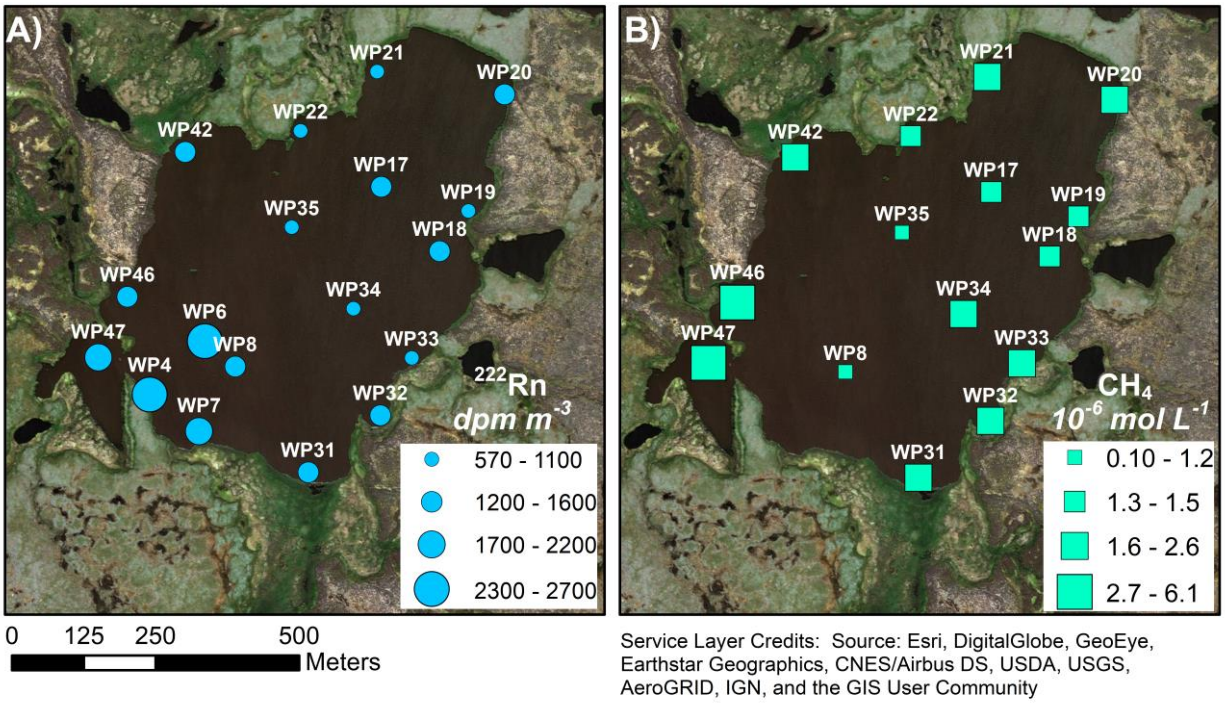

Fig. 2 Concentrations of (a) dissolved ^{222}Rn and (b) dissolved methane in Landing Lake. Sizes of symbols represent relative concentrations. CH_4 error = 30% for all samples; ^{222}Rn error = 16% for WP4, 0.1-6% for all other samples. (Figure was made using ArcMap 10.5.1).

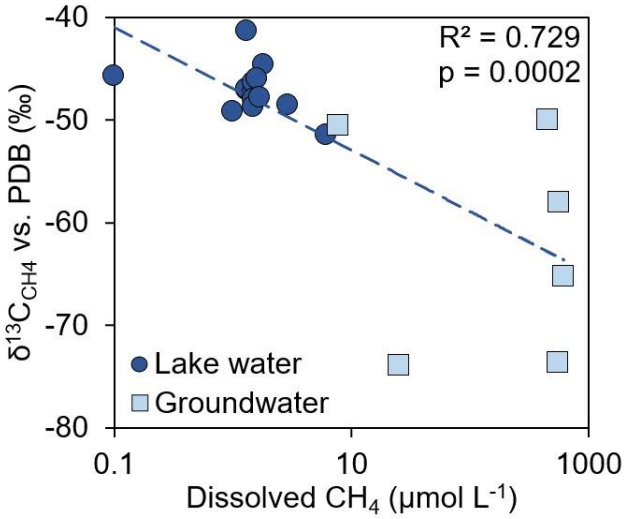

Fig. 3 Stable carbon isotopes of dissolved CH_4 as a function of CH_4 concentration in groundwater (light blue squares) and surface water samples (dark blue circles) at Landing Lake in 2017. Notice the logarithmic scale on the x-axis. The regression equation is $\delta^{13}C = -5.98 \log [CH_4, \mu mol\ L^{-1}] - 46.9‰$ and includes both the lake waters and groundwaters. PDB = Pee Dee Belemnite standard. (Figure made using Microsoft Excel).

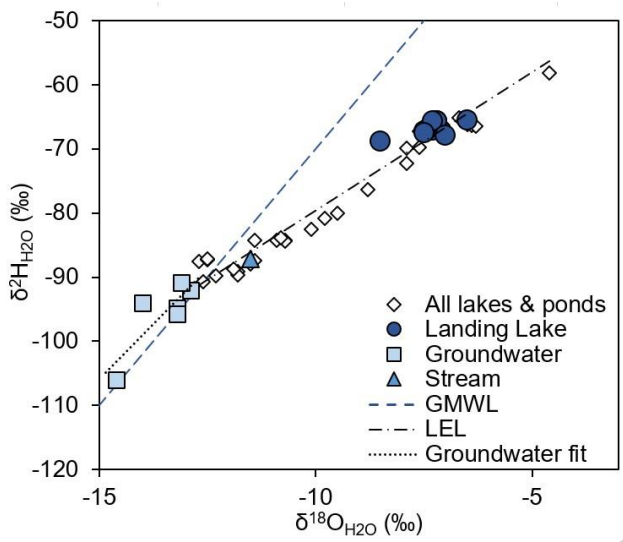

Fig. 4 The stable isotope values for δ^2H and $\delta^{18}O$ in water for samples collected in 2017. The stream sample (triangle) drains Landing Lake. The dashed line is the Global Meteoric Water Line (Craig 1961). Diamonds represent all lake and pond samples collected in 2017 (see data online: (Ludwig et al. 2017b)) which were fit with a Local Evaporation Line (LEL): $\delta^2H_{H2O} = 4.31(\delta^{18}O) - 36.55‰$ ($R^2 = 0.96$, $p << 0.01$). The dotted black line is the best-fit line for Landing Lake groundwaters: $\delta^2H_{H2O} = 6.87(\delta^{18}O) - 2.90‰$ ($R^2 = 0.70$, $p = 0.04$). (Figure made using Microsoft Excel).

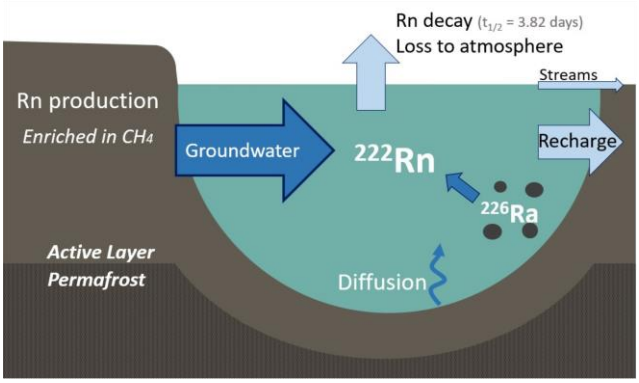

Fig. 5 A conceptual model showing the sources and sinks of ^{222}Rn in Landing Lake. Sources (dark blue arrows) include decay of dissolved ^{226}Ra in lake water, diffusion from lake bottom sediments and groundwater. Sinks (light blue arrows) include ^{222}Rn decay, loss to the atmosphere via gas exchange, recharge into soils, and the stream outlet. (Figure made using Microsoft Powerpoint).

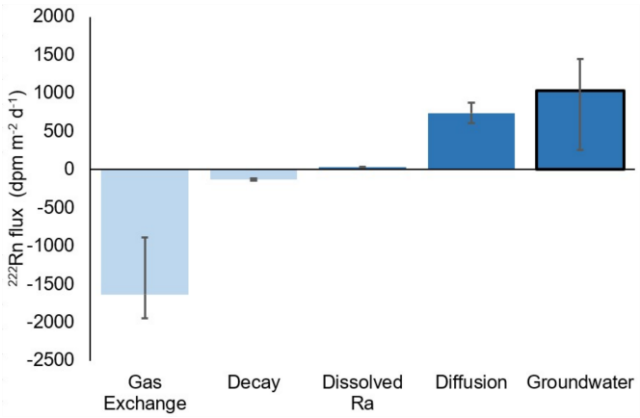

Fig. 6 The fluxes of ^{222}Rn for each source (dark blue) and sink (light blue) in the mass balance model for Landing Lake. The radon flux due to groundwater is highlighted with a black outline because it is the difference between the sinks and the other two sources. Error bars are propagated errors. Lower limits are the conservative estimate discussed in the text. (Figure made using Microsoft Excel).